Mechanical Low-Pass Filtering of Cells for Detection of Circulating Tumor Cells in Whole Blood

Suzuki, Taiki
Department of Biomolecular Engineering, Graduate School of Engineering and ImPACT Research Center for Advanced Nanobiodevices, Nagoya University

Kaji, Noritada
JST, PRESTO

Yasaki, Hirotoshi
Department of Biomolecular Engineering, Graduate School of Engineering and ImPACT Research Center for Advanced Nanobiodevices, Nagoya University

Yasui, Takao
JST, PRESTO

他

出版情報：Analytical Chemistry. 92 (3), pp.2483-2491, 2020-01-10. American Chemical Society
バージョン：

Mechanical Low-Pass Filtering of Cells for Detection of Circulating Tumor Cells in Whole Blood

Taiki Suzuki[†‡], Noritada Kaji[*§//], Hirotoshi Yasaki[†‡], Takao Yasui[†‡§], Yoshinobu Baba[†‡⊥#]

[†]Department of Biomolecular Engineering, Graduate School of Engineering, Nagoya University, Furo-cho, Chikusa-ku, Nagoya 464-8603, Japan

[‡]ImPACT Research Center for Advanced Nanobiodevices, Nagoya University, Furo-cho, Chikusa-ku, Nagoya 464-8603, Japan

[§]JST, PRESTO, 4-1-8 Honcho, Kawaguchi, Saitama, 332-0012, Japan

[//]Department of Applied Chemistry, Graduate School of Engineering, Kyushu University, 744 Motooka, Nishi-ku, Fukuoka 819-0395, Japan

[⊥]Health Research Institute, National Institute of Advanced Industrial Science and Technology (AIST), Hayashi-cho 2217-14, Takamatsu 761-0395, Japan

[#]School of Pharmacy, College of Pharmacy, Kaohsiung Medical University, 100, Shih-Chuan 1st Rd., Kaohsiung, 807, Taiwan, R.O.C.

ABSTRACT: The detection of circulating tumor cells (CTCs) from liquid biopsies using microfluidic devices is attracting a considerable amount of attention as a new, less-invasive cancer diagnostic and prognostic method. One of the drawbacks of the existing antibody-based detection systems is the false negatives for epithelial cell adhesion molecule detection of CTCs. Here, we report a mechanical low-pass filtering technique based on a microfluidic constriction and electrical current sensing system for the novel CTC detection in whole blood without any specific antigen-antibody interaction or biochemical modification of the cell surface. The mechanical response of model cells of CTCs, such as HeLa, A549, and MDA-MB-231 cells clearly demonstrated different behaviors from that of Jurkat cells, a human T-lymphocyte cell line, when they passed through the 6-μm wide constriction channel. A 6-μm wide constriction channel was determined as the optimum size to identify CTCs in whole blood with an accuracy greater than 95% in tens of milliseconds. The mechanical filtering of cells at a single cell level was achieved from a whole blood without any pretreatment (e.g. dilution of lysing) and pre-labeling (e.g. fluorophores or antibodies).

Circulating tumor cells (CTCs), which are shed from the primary tumor and then circulate through the bloodstream, may colonize other organs and cause secondary metastasis. Therefore, understanding metastasis development in cancer patients and the real-time monitoring of cancer therapies and prognoses using CTC-based "liquid biopsies"[1] are essential. The detection and molecular characterization of CTCs is one of the most active areas of translational cancer research, and a number of techniques to enrich and detect CTCs from blood samples are being developed. One of the major challenges is to detect a few CTCs in the approximately 10 million leukocytes and 5 billion erythrocytes that are present in 1 mL of blood. Two approaches exist for CTC detection and enrichment, which are based on biochemical and physical interactions, respectively. The first approach based on biochemical interaction is an immunological procedure using antibodies against the biomarkers of CTCs, including epithelial cell adhesion molecule (EpCAM), cytokeratins (CKs), and CD45 (for negative selection), which has a specificity advantage for detecting and capturing CTCs and is commercially available as CELLSEARCH® CTC Test (Menarini Silicon Biosystems, Italy) [2-4]. Another technique called MagSweeper, developed by an interdisciplinary team of Stanford researchers, uses magnetic rods covered with removable plastic sleeves[5]. An array of anti-EpCAM antibody-coated microposts or columns of self-assembled biofunctionalized superparamagnetic beads in a microfluidic format offered high-throughput selection and capture for genetic analysis[6]. Identification of CTCs from epithelial non-tumor cells and EpCAM-negative cells is exceptionally difficult based on the current epithelial cell-specific EpCAM antibody-based techniques. Hence, various other epithelial cell surface antigens, including human epidermal growth factor receptor 2 (HER2), mucin-1 (MUC1), epidermal growth factor receptor (EGFR), and folate-binding protein receptor (TROP-2) were applied[7]. In contrast to these techniques based on biochemical interactions, physical or mechanical procedures demonstrated lower specificity. However, the main advantage of a physical approach is that it is a non-labeling method; there is no chemical or genetic modification prior to or during the detection and enrichment processes. Density gradient centrifugation (i.e., OncoQuick, Greiner Bio-One, Tokyo, Japan), filtration through specially designed filters[8], an acoustic flow cytometer[9,10], flow fractionation by multiorifice structures in a microfluidic channel[11], and dielectrophoresis field-flow fractionation are typical examples of CTC isolation

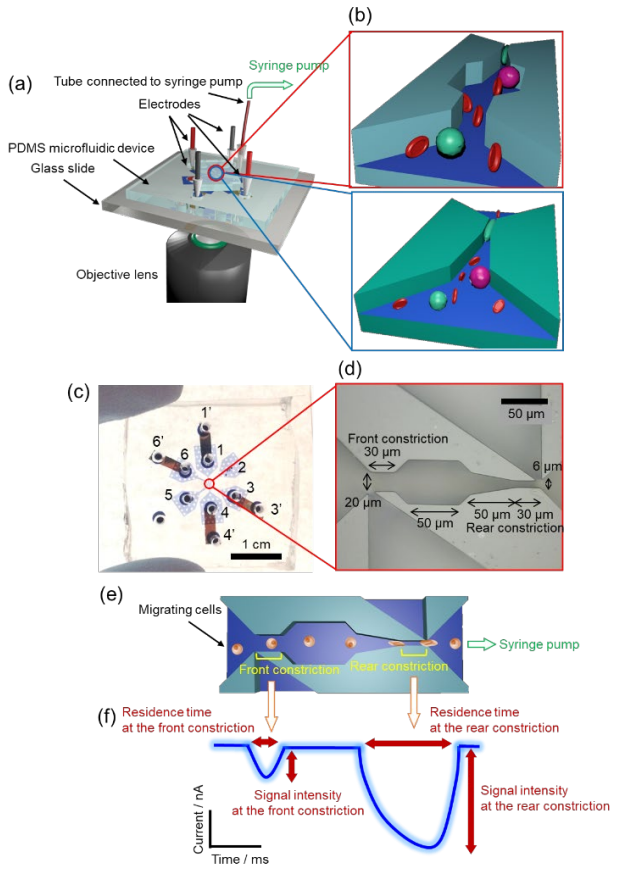

Figure 1. Graphical overview of the experimental setup of the mechanotyping device based on an electrical detection system. (a) A device, electrodes, a tube for withdrawing solution, a glass slide, and an objective lens for direct observation. (b) Close-up graphical images of the two consecutive constriction channels (red frame) and the single constriction channel (blue frame). (c) Image of the mechanotyping device comprised of PDMS microfluidic channels and a glass slide with Au sputtered electrodes. The numbers in black indicate the reservoirs. Reservoirs 1, 3, 4, and 6 are for electrical conduction, reservoir 5 is for sample introduction, and reservoir 2 is for syringe pump connection through the silicone tube to supply the solution. The syringe pump was withdrawn to hydrodynamically drive cells into the detection area. The reservoirs 1', 3', 4', and 6' are for the external Pt electrode insertion. (d) Microscopic image of the consecutive constriction channel. The dimensions of the channel are depicted in the image. (e) Diagram of the detection scheme in the mechanotyping device. When a cell migrates through the front and rear constrictions, the corresponding electrical signals are obtained as depicted in (f).

based on size[12]. Tagging CTCs with a large number of 3-μm microbeads conjugated with anti-EpCAM antibodies by means of Taylor-Gortler vortex-mixing flows is a unique chemical and physical hybrid technique[13].

Here, we report a new non-labeling CTC detection technique in whole blood based on the cell stiffness in a microfluidic constriction channel using an electrical current sensing system developed by our group[14-17]. Magnetic drive peak force modulation atomic force microscope (AFM)[18] and optical tweezers[19] precisely measure the elasticity, viscosity, and plasticity of a cell; however, the techniques are technically difficult, labor intensive, and exhibit a low throughput. The microfluidic format is an alternative technique for high throughput evaluation of the physical properties of cells, although accuracy and precision still need to be addressed. However, many successful results are being reported of a new mechanotyping device to enrich, separate, and isolate the target cells[10,20]. In our previous work, a combination of wide and narrow consecutive constriction channels and an ionic current sensing system for millisecond cell sizing and cell deformability measurement was demonstrated[21]. The ionic current was reduced when a cell passed through the constriction channel, and the intensity of the ionic current at the wide constriction reflected the volume of the migrating cell, while the residence time of the migrating cell at the narrow constriction provided the deformability of the cell. We applied this consecutive constriction device to distinguish CTCs from blood cells based on the differences in the mechanical properties. The results suggest that even a single constriction could identify CTCs in whole blood with almost 95% accuracy. Using this CTC detection method, the current signals and the residence time derived from massive amounts of blood cells at the constriction were sufficiently small in comparison with the model CTCs, and the constriction served as a mechanical low-pass filter.

EXPERIMENTAL SECTION

Device fabrication. Polydimethylsiloxane (PDMS)-based microfluidic devices were fabricated using standard soft lithography methods[22]. Photolithographic masks for patterning the microfluidic channels were delineated using a maskless lithography system (D-light DL-1000GS/NC, Nanosystem Solutions, Inc., Tokyo, Japan) on a mask blank (CBL4009Bu-AZP, Clean Surface Technology Co., Kanagawa, Japan). A negative photoresist (SU-8 3025, Nippoin Kayaku Co. Ltd., Tokyo, Japan) was spin-coated (IF-D7, Mikasa Co., Ltd., Tokyo, Japan) onto a 20 μm thick film following the procedure provided by the supplier. After pre-baking for 10 min at 95 °C, the photoresist was cured by UV exposure through the photolithographic mask using a standard lithography mask aligner (M-1S, Mikasa Co., Ltd., Tokyo, Japan), and then post-baked for 3 min at 95 °C. The cured pattern was developed using SU-8 Developer (Nippon Kayaku Co., Ltd., Tokyo, Japan) and washed with isopropanol (Wako Pure Chemical Industries, Ltd, Tokyo, Japan). The fabricated master mold was silanized in a desiccator, which was filled with trichloro(1H,1H,2H,2H-perfluorooctyl)silane (Sigma-Aldrich Co. LLC., Tokyo, Japan) vapor prior to the addition of a mixture of a curing agent and PDMS prepolymer (SYLGARD 184 Silicone Elastomer Kit, Dow Corning Toray Co., Ltd., Tokyo, Japan) in a 1:10 weight ratio. The prepolymer mixture was degassed in a vacuum desiccator for 2 h and then cured for 2 h at 80 °C. The PDMS replica was peeled from the master, and reservoirs with diameters of 1 mm for tubing connected to a syringe pump, 3 mm for electrodes, and a sample inlet were punched. The surface of the PDMS replica was treated using soft plasma etching equipment (SEDE-PFA, Meiwafosis Co., Ltd., Tokyo, Japan) for 90 s at 5 mA, and then bonded with slide glass for 30 s at 180 °C (Fig. 1a). Gold electrodes of 40 nm thick were deposited onto the slide glass by rf magnetron sputtering (MSP-mini, Vacuum Device, Co., Ltd., Mito, Japan) before bonding.

Cell culture. HeLa cells (a cervical carcinoma cell line), A549 cells (a pulmonary epithelial cell line), and MDA-MB-231 cells (a breast tumor cell line) were cultured at 37 °C in 5% CO_2 in Dulbecco's Modified Eagle's Medium–high glucose (DMEM, D5671, Sigma Aldrich Co. LLC., Tokyo, Japan). Jurkat cells (a human T-cell lymphoma cell line) were cultured under the same conditions in Roswell Park Memorial Institute 1640 Medium (RPMI1640, 11875093, Thermo Fisher Scientific Inc., Tokyo, Japan). Both media were supplemented with a 1% penicillin/streptomycin antibiotic mixture and 10% fetal bovine serum (FBS), which was heat inactivated at 56 °C for 30 min before use.

When HeLa, A549, and MDA-MB-231 cells cultured in 25 cm^3 culture flasks were near-confluent, they were treated with trypsin solution 10× (Sigma Aldrich Co., LLC.) for 3 min; the suspended cells were then collected in a 15 mL conical tube and centrifuged for 3 min at 1000 rpm. The cell pellets were resuspended in the culture medium at an adequate concentration for subculture or the following mechanotyping experiments. The Jurkat cells were cultured and treated using the same conditions as those for the HeLa cells without the trypsin treatment.

Ionic current detection system. A system for the simultaneous detection of an ionic current and optical signal has been developed in our lab, and the system setup is described in detail elsewhere[15-17,23]. In brief, the device consists of two power supplies for electrophoresis and ionic current detection, an ammeter, 1-kΩ resistive elements (e-Globaledge Corporation, Tokyo, Japan), and a variable-resistance element (Multi-Turn Precision Potentiometers, BI Technologies Japan Ltd., Tokyo, Japan). These components were connected to a lead, and comprise the electrical circuit depicted in Figures 1a and 2b. Prior to voltage being applied for electrophoresis, the variable-resistance element in the detection circuit was adjusted to 0 A, which results in no current flow into the detection circuit before measurements. As a cell passes through the detection channel, the resistance in the detection channel increases and the current bypasses the detection channel through the detection circuit. The current and duration are proportional to the cell volume and resident time in the detection channel, respectively, as verified by the experiments. In a conventional series circuit, a constant current (from a few hundred nA to μA level) flows in the detection area and generates Joule heating, which is also directly connected to an Ampere meter. This thermal fluctuation disorders the ion migration in the microchannel filled with buffer that have relatively high ionic strength and high conductivity (~1.6 S/m), and as a result, causes the high background noise. The bridge circuit can reduce this thermal fluctuation because almost no current flows into the Ampere meter on the bridge circuit when the detection area has no sample as illustrated in Figure 2e and 2g. A small part of the electrophoretic current makes a detour along the bridge circuit and detected by the Ampere meter when the sample enters into the detection area as illustrated in Figure 2f. So the background noise was dramatically decreased without losing a signal intensity and response time. For this cell measurement, electrophoresis alone was insufficient to draw cells into the constriction channel; therefore, a syringe pump (KDS200, KD Scientific, Massachusetts, USA) was connected to a reservoir through a silicone tube, as illustrated in Figure 1a, and operated in withdrawal mode to hydrodynamically drive the cells. Prior to the measurements, the buffer conductivity was

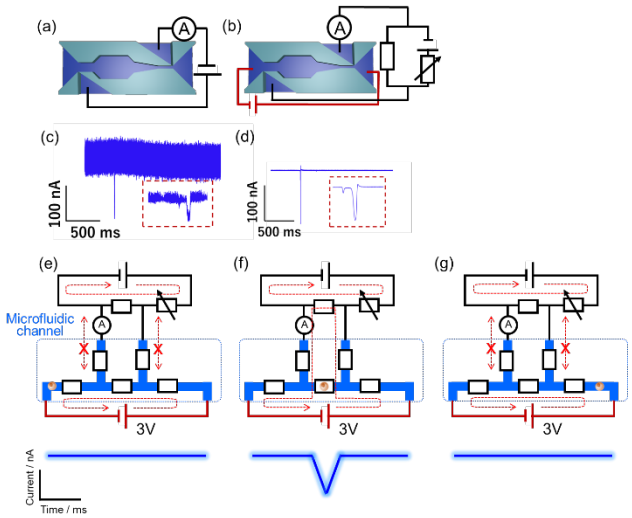

Figure 1. A comparison of (a) a conventional series circuit and (b) a bridge circuit, and typical examples of the electrical signals obtained by (c) a series circuit and (d) a bridge circuit. In the series circuit, the signal was almost buried by the high level of background noise (~100 nA); however, an excellent signal-to-noise ratio was achieved by the bridge circuit. (a) In the series circuit, a constant electric field was applied across the detection area and the electrical signals were obtained when the cell passed through the area by hydrodynamic flow. (b) In a bridge circuit, a constant electric field, as depicted in red, was applied across the detection area to maintain an electrical steady state for current measurement, while the cell was driven into the detection area by hydrodynamic flow. (e-g) Current flow in the bridge circuit and the corresponding current fluctuation caused by the cell passing through the detection area. The current flow and the microchannels filled in solution was depicted in dotted arrow and bold blue line, respectively.

measured using a benchtop conductivity meter (DS-52, Horiba, Ltd., Kyoto, Japan) as shown in Table S1 and used for calculation of the diameters of cells and microparticles. The microchip connected to the electrical circuit was placed on an inverted microscope (Eclipse Ti, Nikon, Tokyo, Japan), and the detection channel was observed during detection of the ionic current.

For fluorescent observation of cells or nuclei, SYTO16 Green Fluorescent Nucleic Acid Stain (Thermo Fisher Scientific Inc., Tokyo, Japan) or Hoechst 33342 (Thermo Fisher Scientific Inc., Tokyo, Japan) were used depending on the microscope setup.

Sample preparation. A contact-activated lancet (Nippon Becton Dickinson Company, Ltd., Japan) was employed to prick a finger of a healthy donor. Immediately thereafter, the blood was drawn into BD Vacutainer K2 EDTA tubes (Nippon Becton Dickinson Company, Ltd., Japan). The whole blood samples used in this study were prepared by suspending HeLa cells in the whole blood at a concentration of 2000 cells/mL.

Ten μL of the sample was introduced into the reservoir and withdrawn by a syringe pump (IC3210, KD Scientific, Holliston, MA) at a flow rate of 3.0 μL/min.

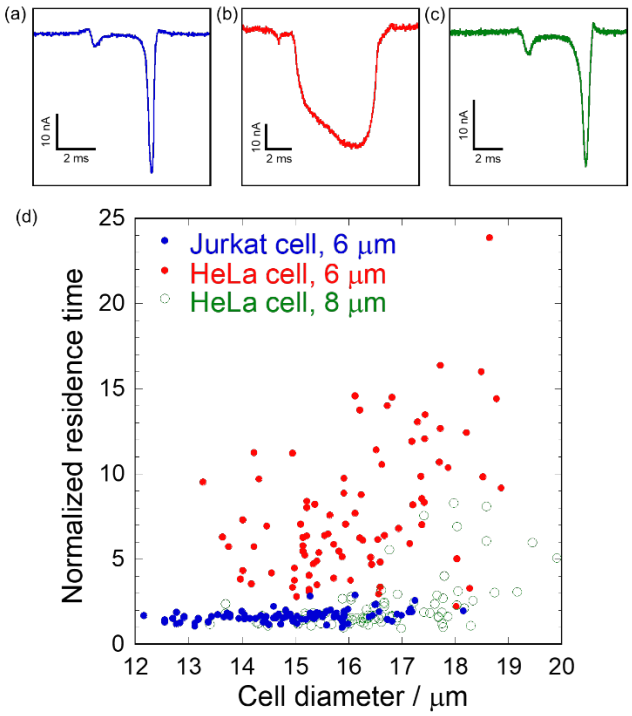

Figure 2. Evaluation of the size and deformability of HeLa and Jurkat cells using two consecutive constrictions with different rear constrictions widths. The typical current signals derived from ion current blockades by (a) a Jurkat cell in the rear constriction channel with a width of 6 μm, (b) a HeLa cell in the rear constriction channel with a width of 6 μm, and (c) a HeLa cell in the rear constriction channel with a width of 8 μm. All front constrictions have the same width of 20 μm, height of 20 μm, and length of 30 μm. (d) The normalized residence times of HeLa and Jurkat cells in rear constriction channels of different sizes as a function of the cell sizes detected at the front constriction channels. (Green circles: HeLa cells, 8 μm rear constriction, N = 90, Blue circles: Jurkat cells, 6 μm rear constriction, N = 98, Red circles: HeLa cells, 6 μm rear constriction, N = 87) The measurement conditions were as follows: DMEM medium with an electric conductivity of 1.548 S/m at 25 °C, 3 V for electrophoresis, and 3 μL/min for hydrodynamic flow.

RESULTS AND DISCUSSION

Constriction channel design. To avoid clogging or damaging the cells at the constriction channel, the threshold pressures at the entrance were estimated in differently shaped channels. By considering the cell as a liquid drop with a constant cortical tension, *Tc*, the threshold pressure can be modeled using the following equation derived from the Laplace-Young equation:

$$\Delta P = T_c\left(\frac{1}{R_a} - \frac{1}{R_b}\right) \qquad (1)$$

where *Ra* and *Rb* are the leading and trailing radii of the liquid drop determined by the channel geometry[24]. If we assume that ΔP is 1 when a cell enters a rectangular constriction channel with 90° corners, ΔP will be 0.8097 and 0.7728 at the tapered channels that have 45° and 10° corners, respectively, as illustrated in Figure S1. Although the extension of the constriction channel accompanying the corner with a smaller angle reduces the sensitivity of the ionic current detection system, the risks of cell clogging and damage are reduced as well and throughput is guaranteed. Therefore, we adopted a tapered channel with 10° corners for all of the following experiments.

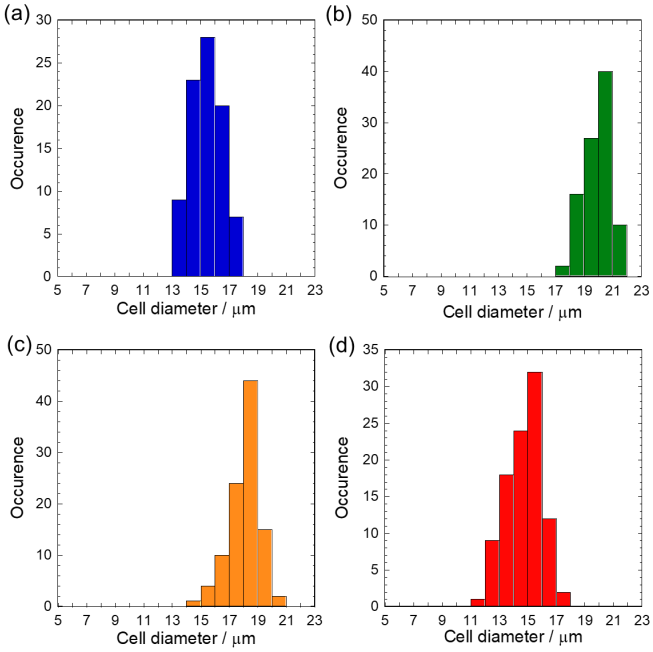

Figure 4. Cell diameters of (a) HeLa, (b) A549, (c) MDA-MB-231, and (d) Jurkat cells measured by the electric current sensing system in two consecutive constriction channels. The width of the front and the rear constrictions are 20 and 10 μm, respectively. The average diameters were (a) 15.485 ± 1.024 (N = 87), (b) 19.936 ± 0.89702 (N = 100), (c) 18.056 ± 1.0417 (N = 100), and (d) 14.766 ± 1.2911 μm (N = 98), respectively. The measurement conditions were as follows: DMEM medium with an electric conductivity of 1.548 S/m at 25 °C, 3 V for electrophoresis, and 3 μL/min for hydrodynamic flow.

Size measurement accuracy. When a cell passes through the constriction channel, a cell-sized volume of conductive solution is extruded, and the resistance of the constriction channel increases due to the lower conductivity of the cell rather than the solution. The ionic current sensing system can detect the current changes and provides information on the cell volume. Here, we validate the accuracy of our sensing system for a size measurement method at a single cell level. First, theoretical calculation was performed based on the assumption that a non-conductive microparticle passes through the constriction channel with a width of 20 μm, 1 of 20 μm, and length of 30 μm, as depicted in Figure S2. The resistance of the constriction channel can be regarded as a series circuit consisting of resistance R_{x1} and R_{x2}, where the microparticle exists or does not exist, respectively. The resistance change, ΔR, can be expressed as the following equation using the resistance of the constriction without the microparticle, R_x:

$$\Delta R = (R_{x1} + R_{x2}) - R_x \qquad (2)$$

The resistance of the constriction channel, R_x, can be expressed as

$$R_x = \frac{\rho L}{WH} \qquad (3)$$

where ρ is the resistivity of the conductive solution and *L, W,* and *H* are the length, width, and height of the constriction channel without the microparticle, respectively. To simplify the calculation, the microparticle is regarded as having the volume of a cube. When a microparticle is introduced into the constriction channel, the resistance will be increased as

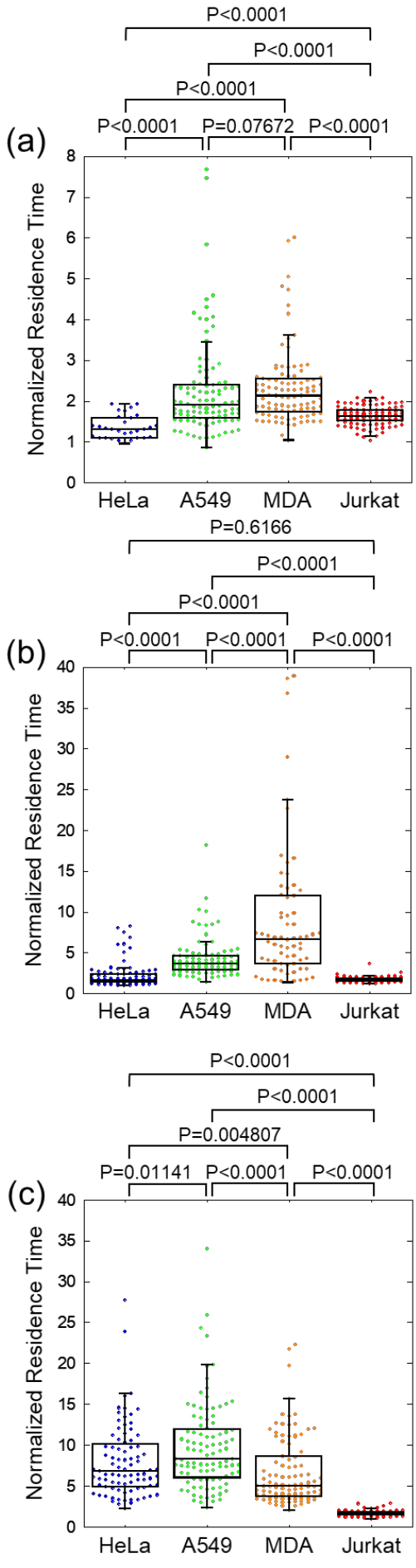

Figure 5. CTC model studies using HeLa, A549, MDA-MB-231, and Jurkat cells. Evaluation of the cell deformability was performed using two consecutive constrictions with rear constrictions of different widths, (a) 10 μm, (b) 8 μm, and (c) 6 μm. (a) Box plots of the normalized residence time of HeLa (N = 30, blue dots), A549 (N = 100, green dots), MDA-MB-231 (N = 99, orange dots), and Jurkat (N = 99, red dots) cells at the rear constrictions (10 μm wide). (b) Box plots of the normalized residence time of HeLa (N = 90, blue dots), A549 (N = 99, green dots), MDA-MB-231 (N = 70, orange dots), and Jurkat (N = 100, red dots) cells at the rear constrictions (8 μm wide). (c) Box plots of the normalized residence time of HeLa (N = 87, blue dots), A549 (N = 100, green dots), MDA-MB-231 (N = 100, orange dots), and Jurkat (N = 98, red dots) cells at the rear constrictions (6 μm wide). The measurement conditions were as follows: DMEM medium with an electric conductivity of 1.548 S/m at 25 °C, 3 V for electrophoresis, and 3 μL/min for hydrodynamic flow.

$$\Delta \boldsymbol{R} = \left(\frac{\boldsymbol{\rho x}}{\boldsymbol{WH - x^2}} + \boldsymbol{\rho}\frac{\boldsymbol{L - x}}{\boldsymbol{WH}}\right) - \frac{\boldsymbol{\rho x}}{\boldsymbol{WH}} \qquad (4)$$

where x is the length of one side of the cube. The current signal intensity, I_{signal}, can be calculated by using a parameter, α, derived from the resistance of the sensing system[14]:

$$\boldsymbol{I_{signal}} = \frac{\boldsymbol{V_{voltage}}}{\boldsymbol{\alpha}}\Delta \boldsymbol{R}$$
$$= \frac{\boldsymbol{V_{voltage}}}{\boldsymbol{\alpha}}\boldsymbol{\rho}\left(\frac{\boldsymbol{x}}{\boldsymbol{WH - x^2}} - \frac{\boldsymbol{x}}{\boldsymbol{WH}}\right) \qquad (5)$$

where $V_{voltage}$ is the voltage of the electrophoretic circuit.

To understand how the migration velocity affects the signal intensity in the current sensing system, the sizes of the microparticles were measured at different flow velocities, as depicted in Figure S3. For 6 μm microparticles, the average detected diameters were 6.08 ± 0.388 μm (N = 100) and 5.99 ± 0.325 μm (N = 100) at 1 μL/min and 5 μL/min, respectively. For 10 μm microparticles, the average detected diameters were 9.88 ± 0.532 μm (N = 100) and 9.78 ± 0.370 μm (N = 100) at 1 μL/min and 5 μL/min, respectively. All the coefficient of variation (CV) was smaller than the CVs provided by the supplier (Polysciences, Inc., Warrington, PA).

Cell size and deformability measurements. In our previous work, a mechanotyping device that has two consecutive constrictions for size and deformability measurements of a single cell was developed (under review). In that device, absolute residence time at the rear constriction for the cell deformability measurements was adopted to evaluate the relationship between cell size and deformability. Hydrodynamic flow fluctuation caused by the syringe pump, water level changes in the reservoir, and intra- and inter-device reproducibility were considered. To exclude the above influences, the residence time at the rear constriction was normalized by the residence time at the front constriction equivalent to the flow velocity. As a result, reproducible deformability measurements were achieved, as illustrated in Figure S4.

In this experiment, we found that the choice of width for the rear constriction channel is critical to enhance the difference in the cell deformability. For example, HeLa and Jurkat cells, which are used as models for solid and blood tumor cells, respectively, were applied to two consecutive constriction channels with a width of 20 and 6 μm in the front and the rear constrictions, respectively. As illustrated in Figure 3(d), the diameters of the Jurkat cells were measured from 12 to 17 μm,

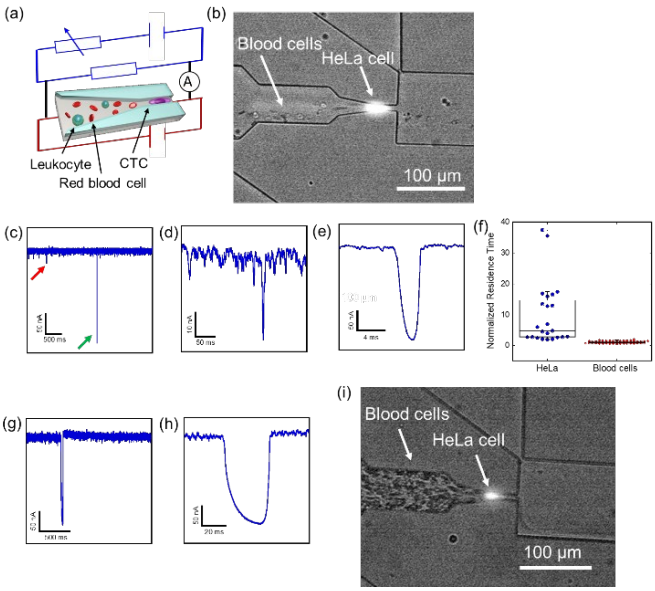

Figure 6. Discrimination of HeLa cells added to whole blood using a single constriction with a width of 6 μm. (a) A graphical image of the CTC discrimination experiment in whole blood by a single constriction device equipped with a bridge electrical circuit. (b) Merged image of bright-field and fluorescent microscope images of a migrating HeLa cell and blood cells at the single constriction site. The whole blood was diluted 10 times by DMEM, and the HeLa cells were stained by SYTO 16 prior to spiking the whole blood samples. (c) A few seconds of a typical current monitoring result. The current signals at the red and green arrows were magnified and shown in (d) and (e), respectively. (f) Box plots of the normalized residence time of HeLa (N = 25) and blood cells (N = 79) in the diluted whole blood samples measured by a single constriction channel. (g) Typical current signal obtained from a non-diluted whole blood sample spiked with HeLa cells and (h) the magnified signal. (i) Merged image of bright-field and fluorescent microscope images of a migrating HeLa cell and non-diluted blood cells at the single constriction site. The measurement conditions were as follows: DMEM medium with an electric conductivity of 1.548 S/m at 25 °C in case of dilution, 3 V for electrophoresis, and 3 μL/min for hydrodynamic flow.

and the normalized residence time was approximately 2 ms despite their sizes. In contrast, the diameters of the HeLa cells were 13–19 μm, slightly larger than the Jurkat cells; however, the normalized residence time was prolonged and widely distributed from a few ms to 25 ms in the 6 μm rear constriction channel. When the channel width of the rear constriction was increased to 8 μm, the signal shape became similar to that in Figure 3(a), and this distribution of the normalized residence time converged to the normalized residence time of the Jurkat cells observed in the 6 μm rear constriction channel, as depicted in Figure 3(d). These results suggest that physical compression can enhance the deformability difference of cells enhance the deformability difference of even cells the same size range. Figure 4 also supports the hypothesis that the normalized residence time is not simply proportional to the size of the cells, as discussed later using other cell types.

Two factors may affect the enhancement: the size of the nucleus[25,26] and the chemical interaction[27,28] between the constriction surface and the cell surface. The average diameters of the nucleus were measured by fluorescent microscope observation. The average diameters were approximately 12 μm and 10 μm in HeLa cells and Jurkat cells, respectively, as depicted in Figure S5. If these small differences in the nucleus size influenced the residence time at the rear constriction, the CTC discrimination from leukocytes may be possible because the tumor cells are reported to develop an enlarged nucleus and are therefore likely to exhibit a greater nucleus to cytoplasm ratio than the leukocytes[29]. In later experiments, we attempted to identify CTCs in whole blood using a single constriction channel. Chemical interactions may also be an important factor affecting the residence time. The surface coating throughout the microchannel was Through Path Plus (On-chip Biotechnologies, Tokyo, Japan), which is widely used to avoid non-specific adsorption of cells onto the chip in chip-based flow cytometry or cell sorting. Size and deformability measurements by two consecutive constrictions were performed. As depicted in Figure S6, the normalized residence time decreased over all cell diameters. However, compared to Jurkat cells, HeLa cells exhibited a longer residence time in the rear constriction. Therefore, if the constriction size was optimized to enhance the cell deformability difference, HeLa and Jurkat cells can be distinguished from just the residence time at the rear constriction. To verify this assumption, the cell deformability of A549 and MDA-MB-231 as a model of CTCs was measured.

Cell size and deformability measurements of A549 and MDA-MB-231 cells. We prepared rear constriction channels with three different widths of 6, 8, and 10 μm and measured the residence time of HeLa, A549, MDA-MB-231, and Jurkat cells. All front constrictions had 20 μm widths and cells' sizes were measured based on the signal intensities. Figure 4 illustrates a histogram of the calculated cell diameters. Jurkat cells were the smallest with a diameter of approximately 15 μm. The normalized residence time of each cell at the rear constrictions is depicted in Figure 5. Statistical analysis was performed using KaleidaGraph software (KaleidaGraph 4.5, HULINKS, Tokyo, Japan). In the 10-μm wide constriction, all the cell types passed the constriction in approximately 2 ms and were statistically significant at the 0.01% level (p-value by Wilcoxon-Mann-Whitney test), except the residence times of the A549 and MDA-MB231 cells. It is interesting that the normalized residence time of MDA-MB-231 became drastically longer when compared to the other cell types in the 8-μm wide constriction, and all the three types of solid tumor cells (HeLa, A549, MDA-MB-231) exhibited longer residence times over 5 ms in the 6-μm wide constriction. In contrast, the normalized residence time of Jurkat cells remained constant at approximately 2 ms, regardless of the constriction width. Therefore, the normalized residence time is not proportional to the cell size and may be determined by multiple factors including nucleus size. There is still some overlap of the normalized residence time of Jurkat cell and the other cells in the 6-μm wide constriction. We hypothesized that highly condensed nucleus at metaphase (M phase) of Jurkat cell might retard the residence time and show the similar residence time of the other cancer cells especially which have loosely packed nucleus at interphase (G1 phase). In a 4-μm wide constriction, all of the cell types were easily clogged and no quantitative data was obtained. One application of the current device would be a high-speed CTC discrimination and counting device in whole blood based on the unique criteria observed in the above experiments.

CTC detection in whole blood using a single constriction device. Based on the above results using two consecutive constrictions, a new device focusing on discrimination of CTCs in whole blood was developed. A single constriction consisting of a 6-μm wide, 20-μm high, and 30-μm long microchannel was fabricated, and a bridge electrical circuit was set as depicted in Figure 6(a). In the first attempt, whole blood from a healthy donor was diluted 10 times with DMEM and HeLa cells were spiked into the diluted whole blood as models of CTCs at the final concentration of 2,000 cells/mL. Prior to spiking the whole blood, the HeLa cells were stained with SYTO16 to confirm the position in the microchannel by fluorescence observation. After the sample was introduced, the electrical current was monitored under a constant flow of 3.0 μL/min and optical observation was performed simultaneously. Figures 6(b) and (c) illustrate an image of a HeLa cell passing through the constriction in blood diluted 10 times and the current signals, respectively. Current signals derived from vast amounts of erythrocytes and leukocytes were likely baseline fluctuations, ~20 mA, as depicted in Figure 6(d), and the normalized residence time was shorter than 1 ms. When a HeLa cell passed through the constriction, strong current signals over 100 mA with a longer residence time of approximately 5 ms were observed, as depicted in Figure 6(e). The box plots in Figure 6(f) demonstrate that the optimized size of the constriction can discriminate CTCs from blood cells based on the normalized residence time as well as the signal intensities. Therefore, the constriction successfully cut off the low intensity and short time signals and picked up the target signals derived from CTCs.

Next, the mechanical low-pass filter was used to detect CTCs in whole blood without any dilution. A whole blood assay, including immunoassay and CTC assay, in a microfluidic device generally requires dilution of the blood sample because of its high viscosity and clogging problem. Although our device rarely encountered clogging issues for long operation times, HeLa cells were successfully discriminated even in whole blood without dilution, as depicted in Figure 6(g–i). This result strongly suggests the potential for high throughput of cell assays for CTC detection in whole blood.

CONCLUSION

A combination of two consecutive constrictions in a microfluidic device, equipped with an electrical current sensing detector, revealed the optimum constriction width to discriminate CTCs from blood cells. By adjusting the constriction width, the signal intensity, and the residence time of CTCs at the constriction channel was enhanced and the signals of the blood cells were cut off. As a result, the device served as a mechanical low-pass filter and enabled high throughput CTC detection with ~95% accuracy even in whole blood without pretreatment or dilution.

ASSOCIATED CONTENT

Supporting Information

The Supporting Information is available free of charge on the ACS Publications website.

Optimization of the corner angle in the constriction channel, theoretical calculation of the current signal intensity, validation of the size measurements, normalization of the residence time, nucleus information, surface coating effects (PDF).

AUTHOR INFORMATION

Corresponding Author

*E-mail: kaji@cstf.kyushu-u.ac.jp

Author Contributions

All authors have given approval to the final version of the manuscript.

Notes

The authors declare no competing financial interest.

ACKNOWLEDGMENT

This work was partially supported by JST/PRESTO [grant number JPMJPR16F4, JPMJPR151B], Grant-in-Aid for Scientific Research on Innovative Areas [18H04545], Nanotechnology Platform Program (Molecule and Material Synthesis) of the Ministry of Education, Culture, Sports, Science and Technology (MEXT), a JSPS Grant-in-Aid for Scientific Research (A) [16H0209], the ImPACT Program of the Council for Science, Technology and Innovation (Cabinet Office, Government of Japan), and a research grant from the Nitto Foundation.

REFERENCES

(1) Alix-Panabieres, C.; Pantel, K. *Clinical Chemistry* **2013**, *59*, 110-118.
(2) Naoe, M.; Ogawa, Y.; Morita, J.; Omori, K.; Takeshita, K.; Shichijyo, T.; Okumura, T.; Igarashi, A.; Yanaihara, A.; Iwamoto, S.; Fukagai, T.; Miyazaki, A.; Yoshida, H. *Cancer* **2007**, *109*, 1439-1445.
(3) Truini, A.; Alama, A.; Dal Bello, M. G.; Coco, S.; Vanni, I.; Rijavec, E.; Genova, C.; Barletta, G.; Biello, F.; Grossi, F. *Frontiers in oncology* **2014**, *4*, 242.
(4) Adams, D. L.; Stefansson, S.; Haudenschild, C.; Martin, S. S.; Charpentier, M.; Chumsri, S.; Cristofanilli, M.; Tang, C.-M.; Alpaugh, R. K. *Cytometry Part A* **2015**, *87*, 137-144.
(5) Talasaz, A. H.; Powell, A. A.; Huber, D. E.; Berbee, J. G.; Roh, K.-H.; Yu, W.; Xiao, W.; Davis, M. M.; Pease, R. F.; Mindrinos, M. N.; Jeffrey, S. S.; Davis, R. W. *Proceedings of the National Academy of Sciences* **2009**, *106*, 3970-3975.
(6) Nagrath, S.; Sequist, L. V.; Maheswaran, S.; Bell, D. W.; Irimia, D.; Ulkus, L.; Smith, M. R.; Kwak, E. L.; Digumarthy, S.; Muzikansky, A.; Ryan, P.; Balis, U. J.; Tompkins, R. G.; Haber, D. A.; Toner, M. *Nature* **2007**, *450*, 1235.
(7) Gabriel, M. T.; Calleja, L. R.; Chalopin, A.; Ory, B.; Heymann, D. *Clinical Chemistry* **2016**, *62*, 571-581.
(8) Zhou, M. D.; Hao, S.; Williams, A. J.; Harouaka, R. A.; Schrand, B.; Rawal, S.; Ao, Z.; Brenneman, R.; Gilboa, E.; Lu, B.; Wang, S.; Zhu, J.; Datar, R.; Cote, R.; Tai, Y. C.; Zheng, S. Y. *Sci Rep* **2014**, *4*, 7392.
(9) Li, P.; Mao, Z.; Peng, Z.; Zhou, L.; Chen, Y.; Huang, P.-H.; Truica, C. I.; Drabick, J. J.; El-Deiry, W. S.; Dao, M.; Suresh, S.; Huang, T. J. *Proceedings of the National Academy of Sciences* **2015**, *112*, 4970-4975.
(10) Karabacak, N. M.; Spuhler, P. S.; Fachin, F.; Lim, E. J.; Pai, V.; Ozkumur, E.; Martel, J. M.; Kojic, N.; Smith, K.; Chen, P.-i.; Yang, J.; Hwang, H.; Morgan, B.; Trautwein, J.; Barber, T. A.; Stott, S. L.; Maheswaran, S.; Kapur, R.; Haber, D. A.; Toner, M. *Nature Protocols* **2014**, *9*, 694.
(11) Moon, H.-S.; Kwon, K.; Hyun, K.-A.; Seok Sim, T.; Park, J.; Lee, J.-G.; Jung, H.-I. *Continual collection and re-separation of circulating tumor cells from blood using multi-stage multi-orifice flow fractionation*, 2013; Vol. 7.
(12) Warkiani, M. E.; Guan, G.; Luan, K. B.; Lee, W. C.; Bhagat, A. A. S.; Kant Chaudhuri, P.; Tan, D. S.-W.; Lim, W. T.; Lee, S. C.; Chen, P. C. Y.; Lim, C. T.; Han, J. *Lab on a Chip* **2014**, *14*, 128-137.
(13) Lin, M. X.; Hyun, K.-A.; Moon, H.-S.; Sim, T. S.; Lee, J.-G.; Park, J. C.; Lee, S. S.; Jung, H.-I. *Biosensors and Bioelectronics* **2013**, *40*, 63-67.

(14) Yasaki, H.; Yasui, T.; Yanagida, T.; Kaji, N.; Kanai, M.; Nagashima, K.; Kawai, T.; Baba, Y. *Journal of the American Chemical Society* **2017**, *139*, 14137-14142.
(15) Yasaki, H.; Yasui, T.; Yanagida, T.; Kaji, N.; Kanai, M.; Nagashima, K.; Kawai, T.; Baba, Y. *Sensor Actuat B-Chem* **2018**, *260*, 746-752.
(16) Yasaki, H.; Yasui, T.; Yanagida, T.; Kaji, N.; Kanai, M.; Nagashima, K.; Kawai, T.; Baba, Y. *Chem Lett* **2018**, *47*, 350-353.
(17) Yasaki, H.; Shimada, T.; Yasui, T.; Yanagida, T.; Kaji, N.; Kanai, M.; Nagashima, K.; Kawai, T.; Baba, Y. *Acs Sensors* **2018**, *3*, 574-579.
(18) Meng, X.; Zhang, H.; Song, J.; Fan, X.; Sun, L.; Xie, H. *Nature Communications* **2017**, *8*, 1944.
(19) Killian, J. L.; Ye, F.; Wang, M. D. *Cell* **2018**, *175*, 1445-1448.
(20) Hou, H. W.; Warkiani, M. E.; Khoo, B. L.; Li, Z. R.; Soo, R. A.; Tan, D. S.-W.; Lim, W.-T.; Han, J.; Bhagat, A. A. S.; Lim, C. T. *Scientific Reports* **2013**, *3*, 1259.
(21) Sano, M.; Kaji, N.; Rowat, A. C.; Yasaki, H.; Shao, L.; Odaka, H.; Yasui, T.; Higashiyama, T.; Baba, Y. *Analytical Chemistry* **2019**. *91*, 12890-12899.
(22) McDonald, J. C.; Duffy, D. C.; Anderson, J. R.; Chiu, D. T.; Wu, H.; Schueller, O. J.; Whitesides, G. M. *Electrophoresis* **2000**, *21*, 27-40.
(23) Yasaki, H.; Yasui, T.; Yanagida, T.; Kaji, N.; Kanai, M.; Nagashima, K.; Kawai, T.; Baba, Y. *J Am Chem Soc* **2017**, *139*, 14137-14142.
(24) McFaul, S. M.; Lin, B. K.; Ma, H. *Lab Chip* **2012**, *12*, 2369-2376.
(25) Rowat, A. C.; Lammerding, J.; Ipsen, J. H. *Biophys J* **2006**, *91*, 4649-4664.
(26) Rowat, A. C.; Bird, J. C.; Agresti, J. J.; Rando, O. J.; Weitz, D. A. *Proceedings of the National Academy of Sciences* **2009**, *106*, 18149-18154.
(27) Kim, J.; Li, B.; Scheideler, O. J.; Kim, Y.; Sohn, L. L. *iScience* **2019**, *13*, 214-228.
(28) Balakrishnan, K. R.; Whang, J. C.; Hwang, R.; Hack, J. H.; Godley, L. A.; Sohn, L. L. *Anal Chem* **2015**, *87*, 2988-2995.
(29) Park, S.; Ang, R. R.; Duffy, S. P.; Bazov, J.; Chi, K. N.; Black, P. C.; Ma, H. *PLOS ONE* **2014**, *9*, e85264.

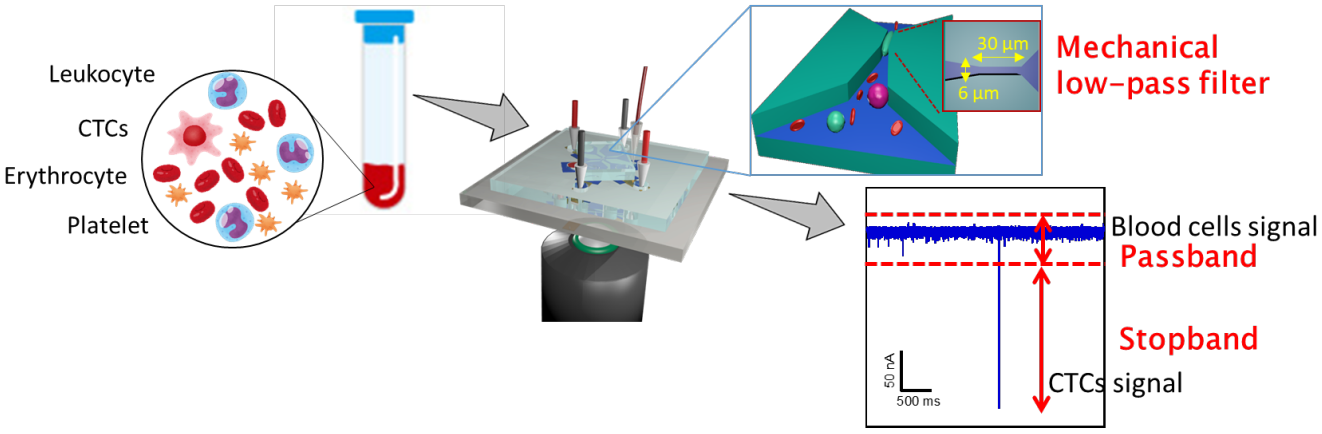

Table of Contents